

## Original Article

**Cite this article:** Deng WB, Shao ZG, Xu HJ, Chen XH, Yi JJ, and Zhang SJ (2023) Geochemistry, zircon U–Pb geochronology and Hf isotope of the early Permian gabbro and high-Mg diorites from the Zhusileng–Hangwula Belt in the northern Alxa area: Petrogenesis and tectonic implications. *Geological Magazine* **160**: 1417–1427. <https://doi.org/10.1017/S0016756823000444>

Received: 9 August 2022

Revised: 10 June 2023

Accepted: 23 June 2023

First published online: 11 August 2023

**Keywords:**



Central Asian Orogenic Belt; Northern Alxa area; high-Mg diorite; early Permian; tectonic setting

**Corresponding author:**

Zhao Gang Shao;

Email: [shaozhaogang@sina.com](mailto:shaozhaogang@sina.com)

# Geochemistry, zircon U–Pb geochronology and Hf isotope of the early Permian gabbro and high-Mg diorites from the Zhusileng–Hangwula Belt in the northern Alxa area: Petrogenesis and tectonic implications

Wen Bing Deng<sup>1,2,3</sup> , Zhao Gang Shao<sup>1</sup> , Hai Jin Xu<sup>2</sup>, Xuan Hua Chen<sup>1</sup>, Jin Jun Yi<sup>3</sup> and Su Jiang Zhang<sup>3</sup>

<sup>1</sup>Chinese Academy of Geological Sciences, Beijing, China; <sup>2</sup>School of Earth Sciences, China University of Geosciences, Wuhan, China and <sup>3</sup>Cores and Samples Center of Natural Resources, China Geological Survey, Sanhe, China

**Abstract**

As the southernmost part of the central segment of the Central Asian Orogenic Belt, the northern Alxa area is characterized by abundant Permian magmatism and records key information on the geological evolution of the Palaeo-Asian Ocean. This study reports new zircon U–Pb and Lu–Hf isotopic and whole-rock geochemical data of the early Permian (285–286 Ma) Huisentala gabbro and Huodonghaer diorites from the Zhusileng–Hangwula Belt in the northern Alxa area. The gabbro is characterized by high Al, Ca, Mg<sup>#</sup> and light rare-earth elements, and low K, P and high field strength elements (e.g., Ti, Nb and Ta). Furthermore, the gabbro shows heterogeneous zircon  $\epsilon_{\text{Hf}}(t)$  value (–2.5 to +2.6). The Huodonghaer diorites show high MgO (3.46–6.32 wt%), Mg<sup>#</sup> (49–58), Sr (408–617 ppm) and Ba (223–419 ppm), and low FeO<sup>T</sup>/MgO (1.27–1.83) and TiO<sub>2</sub> (0.48–0.90 wt%), with geochemical features similar to the high-Mg andesite/diorite. They show radiogenic zircon  $\epsilon_{\text{Hf}}(t)$  values of +1.2 to +4.9 and high Th/Nb ratios. These features suggest that the Huisentala gabbro and the Huodonghaer diorites were derived from the partial melting of mantle peridotite that was metasomatized by subduction-related fluids and by subducted sediment-derived melts, respectively.

**1. Introduction**

The Central Asian Orogenic Belt (CAOB), one of the largest accretionary orogens in the world, is bounded by the Eastern European Craton to the east, the Tarim Craton and North China Craton to the south and the Siberia Craton to the north (Fig. 1a, Şengör *et al.* 1993; Windley *et al.* 2007; Wilhem *et al.* 2012; Xiao *et al.* 2013). The complicated accretionary processes and considerable continental crustal growth of the CAOB from ca. 1000 to 250 Ma were associated with the consumption of the Palaeo-Asian Ocean (PAO) (Hong *et al.* 2004; Jahn *et al.* 2004; Xu *et al.* 2013; Eizenhöfer *et al.* 2014; Xiao *et al.* 2018). The northern Alxa area plays a significant role to constrain the tectonic and crustal evolution of the southern CAOB (Fig. 1a). The northern Alxa area is characterized by the widespread development of late Palaeozoic plutons (Zhang *et al.* 2016, 2017; Liu *et al.* 2018a, b; Fei *et al.* 2019; Li *et al.* 2020; Shi *et al.* 2020; Song *et al.* 2020; Zhao *et al.* 2020). However, its tectonic setting during the late Palaeozoic is still debated. Previous researchers argued that the central PAO closed before the early Permian (Fei *et al.* 2019; Li *et al.* 2020), and the northern Alxa area underwent post-collisional extension during the late Palaeozoic, while other scholars suggested that ocean subduction was still active during the late Palaeozoic, and the central PAO closed in the early Triassic (Song *et al.* 2020; Xie *et al.* 2021).

The northern Alxa area, as the southernmost part of the central segment of the CAOB, is located at a crucial junction between the Solonker Suture and the Central Tianshan Arc and the Beishan Orogenic Belt (Fig. 1b). In this study, we present new geochronological, geochemical and zircon Hf isotopic data for the early Permian gabbro and diorites from the Zhusileng–Hangwula Belt in the northern Alxa area. These results, combined with published data, are used to discuss the petrogenesis of the igneous rocks and tectonic setting and to reconstruct the geological evolutionary history of the central part of the southern CAOB during the late Palaeozoic.

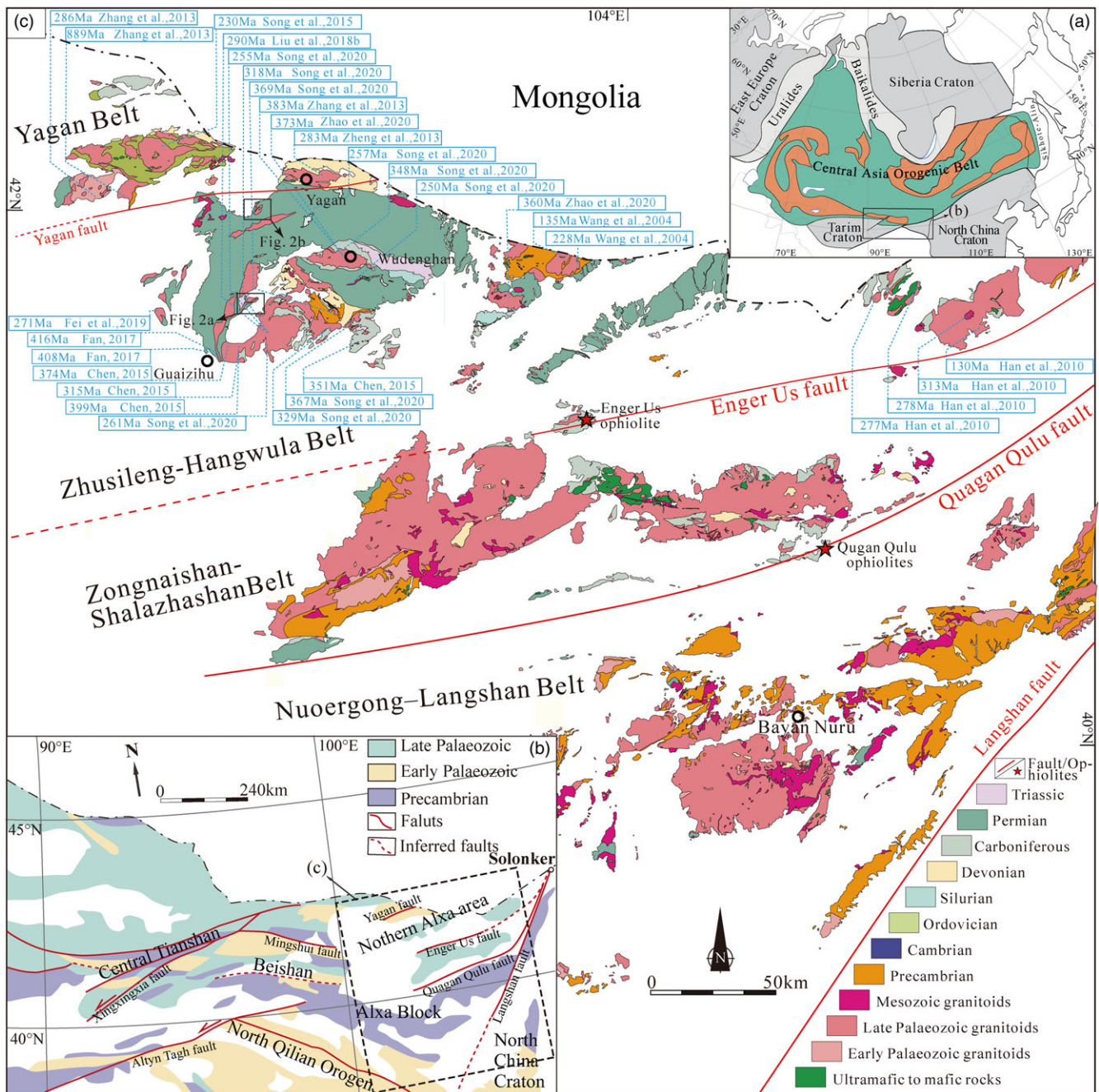


**Figure 1.** (Colour online) (a) The Location of the northern Alxa area in the simplified tectonic sketch map of the Central Asian Orogenic Belt (CAOB) (Modified after Eizenhöfer *et al.* 2014). (b) Tectonic outline of the southern CAOB in north China (after Chen *et al.* 2019). (c) Geological map of the northern Alxa area and adjacent tectonic units (modified after Liu *et al.* 2018a).

## 2. Geological setting and samples

The northern Alxa area, the southernmost segment of the CAOB, is divided into two parts by the Yagan fault: from north to south, the Yagan Belt and the Zhusileng–Hangwula Belt (Fig. 1a). Two important faults, the Enger Us fault and the Quagan Qulu fault, are characterized by ophiolitic mélanges (Fig. 1b; BGMIRM, 1991; Wu & He, 1993; Wu *et al.* 1998).

The Quagan Qulu fault separates the Zongnaishan–Shalazhashan Belt and the Nuorgong–Langshan Belt (Fig. 1b). The Nuorgong–Langshan Belt is mainly composed of Precambrian basement rocks

and late Palaeozoic magmatic rocks (321–265 Ma). As shown in recent studies (Geng & Zhou, 2012; Wang *et al.* 2016, 2021; Zheng *et al.* 2018; Zheng *et al.* 2019), the Precambrian rocks comprise Palaeoproterozoic gneisses and amphibolites, with small amounts of Neoproterozoic granites (970–880 Ma), and the Phanerozoic rocks are mainly composed of granites, diorites and minor gabbro (321–265 Ma). By comparison, 301–247 Ma magmatic rocks and late Palaeozoic sediments, with some Mesozoic granites, dominate in the Zongnaishan–Shalazhashan Belt (Shi *et al.* 2014; Zheng *et al.* 2014; Song *et al.* 2017). A few Precambrian metamorphic rocks with ages of



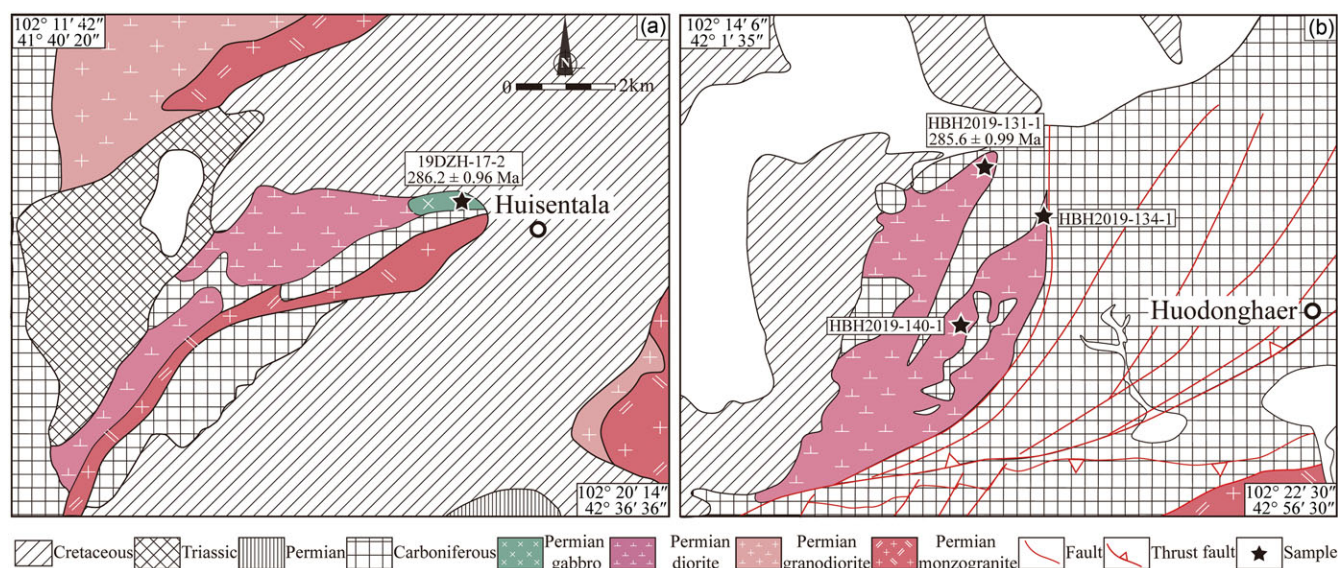


**Figure 2.** (Colour online) Geological maps showing sampling locations and ages. (a) Huisentala area (modified after the 1: 200,000 geological maps from BGMIR, 1991). (b) Huodonghaer area (after the 1: 200,000 geological maps from BGMIR, 1991).

1.5–1.4 Ga have also been reported (Qing, 2010; Song, 2014; Shi *et al.* 2016; Wang *et al.* 2019), indicating that the tectonic affinity of the Zongnaishan–Shalazhashan Belt, which was treated as a part of the Alxa Block, was uncertain given the occurrence of Mesoproterozoic rocks in the Zongnaishan area.

The Yagan Belt mainly contains Palaeozoic volcano-sedimentary strata (Wu & He, 1993) and plutons (397–220 Ma; Zheng *et al.* 2013; Liu *et al.* 2018a), with some Neoproterozoic granite (Zhang *et al.* 2016). Based on litho-tectonic comparisons, the Yagan and Zhusileng–Hangwula Belts have been generally considered the eastern extension of the Beishan Orogenic Belt (Wu *et al.* 1998).

The Zhusileng–Hangwula Belt is characterized by widespread Palaeozoic to Mesozoic volcano-sedimentary formations and magmatic rocks as well as minor Precambrian rocks (BGMIR, 1991; Wu & He, 1993; Yin *et al.* 2015). The Mesoproterozoic–early Neoproterozoic rocks (1400–916 Ma) are sporadically exposed in the region (Wang *et al.* 2002; Zhou *et al.* 2013; Deng *et al.* 2022a; Yu *et al.* 2022). The early Palaeozoic strata only include Cambrian limestone, late Ordovician limestone and early Silurian siliceous rocks. Late Palaeozoic strata are composed of clastic rocks, limestone and minor volcanic rocks, which are unconformably overlain by late Triassic and Cretaceous continental clastic sediments (Chen *et al.* 2019). The Phanerozoic intrusions in the Zhusileng–Hangwula Belt were generated during the middle–late Devonian (399–373 Ma), late Carboniferous–middle Permian (325–263 Ma) and middle–late Triassic (250–216 Ma), including gabbro, diorite, granodiorite, granite and monzogranite (Fig. 1c; Wang *et al.* 2002; Li, 2006; Han *et al.* 2010; Dang *et al.* 2011; Chen, 2015; Zhang *et al.* 2017; Liu *et al.* 2018a; Shi *et al.* 2018; Chen *et al.* 2019; Li *et al.* 2020; Song *et al.* 2020; Deng *et al.* 2022b, 2023, b; Fei *et al.* 2019; Zhao *et al.* 2020).

For this study, samples of gabbro and diorites were examined, and sample locations can be found in Fig. 2. The Huisentala gabbro (19DZH-17-2) is black and grey-coloured, moderate- to coarse-grained and is mainly composed of plagioclase (~60%), hornblende (~20%), biotite (~15%) and minor quartz (~5%) (Fig. 3a). The Huodonghaer diorites, intruded by granodiorite, show dark green colour and moderate to coarse-grained texture (Fig. 3b). They are strongly weathered and mainly consist of plagioclase

(~75%), hornblende (~10%), biotite (~10%) and minor quartz (~5%) (Fig. 3c).

### 3. Analytical methods

#### 3.a. Zircon U–Pb dating

After crushing, zircon crystals were extracted using heavy liquid and magnetic techniques. Zircons were hand-picked and mounted in epoxy resin and polished to about half of their size to expose the core of the grain. The detailed procedure can be found in Song *et al.* (2002). The cathodoluminescence (CL) images of zircon were obtained using a scanning electron microscope (IT-500, Japan) at Beijing Geoanalysis Co., Ltd (Beijing, China). Analytical spots for U–Pb dating were chosen after combined studies of transmitted and reflected light microscope and CL images. Laser ablation inductively coupled plasma-mass spectrometry (LA-ICP-MS) zircon U–Pb analyses were carried out using an Agilent 7900 ICP-MS equipped with a 193-nm laser ablation system at the Institute of Geology, Chinese Academy of Geological Sciences in Beijing, China. The detailed procedure is the same as described by Hou *et al.* (2007). Zircon 91500 and GJ-1 were used as primary and secondary standards for U–Pb dating, respectively (Jackson *et al.* 2004). ISOPLOT 3.0 was used to plot the concordia diagrams and perform the weighted mean calculations (Ludwig, 2003). Uncertainties are quoted at 2 $\sigma$  level for individual analysis, and the weighted mean ages are given at the 95% confidence level.

#### 3.b. Zircon Lu–Hf isotopic analyses

Zircon Hf isotope analyses were conducted using a multiple collector inductively coupled plasma-mass spectrometer (MC-ICP-MS, Neptune Plus, Thermo Fisher Scientific, Germany) equipped with a femtosecond ( $\lambda = 343$  nm) laser-ablation system (J-200, Applied Spectra, USA) at the National Research Center for Geoanalysis in Beijing. To evaluate the quality of the data, Temora and Plesovice zircon were used as the standards and exhibited  $^{176}\text{Hf}/^{177}\text{Hf}$  ratios of  $0.282692 \pm 0.000018$  (2 $\sigma$ ,  $n = 15$ ) and  $0.282480 \pm 0.000021$  (2 $\sigma$ ,  $n = 49$ ), respectively. The analytical details and interference correction



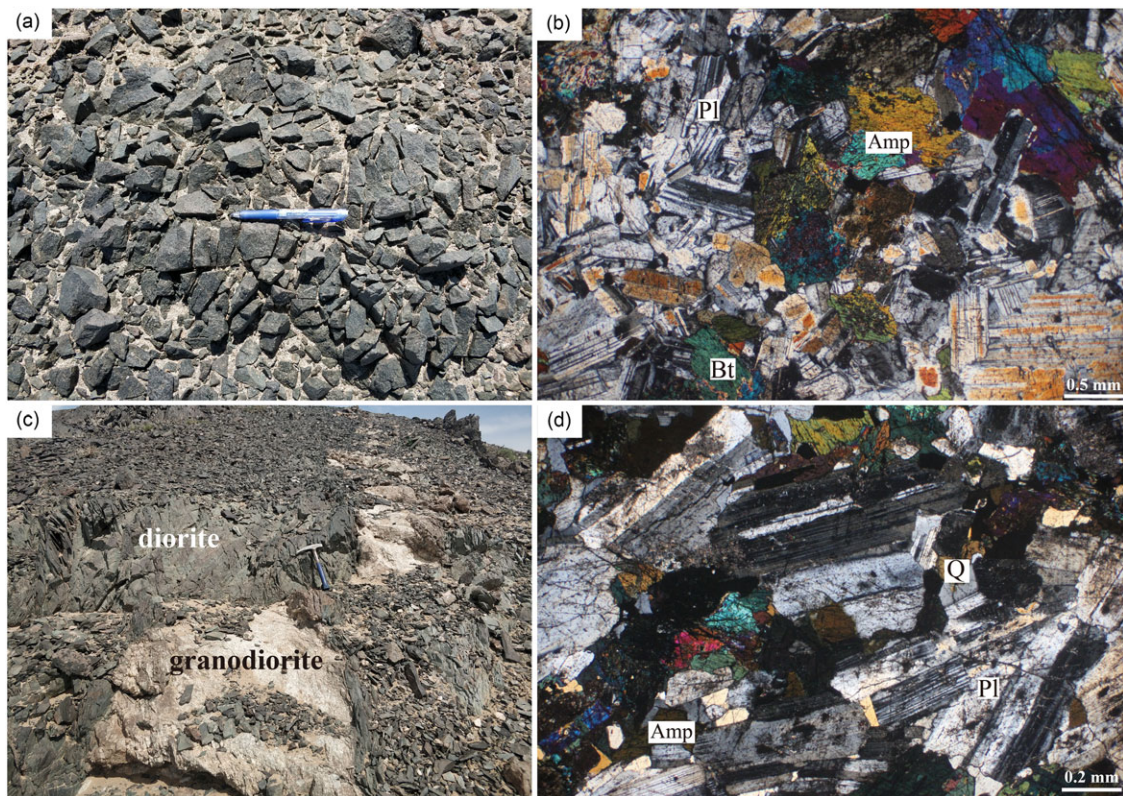


**Figure 3.** (Colour online) Representative outcrops and microphotographs of investigated gabbro and diorites from the Zhusileng–Hangwula Belt. (a) and (b) Gabbro (sample 19DZH-017-2). (c) and (d) Diorite (sample HBH2019-131-1). Amp, Amphibole; Bt, Biotite; Pl, Plagioclase; Qtz, quartz.

method of  $^{176}\text{Yb}$  on  $^{176}\text{Hf}$  can be found in Zhou *et al.* (2018) and Wu *et al.* (2006), respectively. The  $^{176}\text{Lu}$  decay constant of  $1.865 \times 10^{-11} \text{ yr}^{-1}$  (Scherer *et al.* 2007) was used to calculate the initial  $^{176}\text{Hf}/^{177}\text{Hf}$  ratios. The chondritic values of 0.0336 and 0.282785 for  $^{176}\text{Lu}/^{177}\text{Hf}$  and  $^{176}\text{Hf}/^{177}\text{Hf}$ , respectively, reported by Bouvier *et al.* (2008), were used for the calculation of the  $\epsilon_{\text{Hf}}$  values. The depleted mantle Hf model ages ( $T_{\text{DM}}$ ) were calculated using the measured  $^{176}\text{Lu}/^{177}\text{Hf}$  ratios based on the assumption that the depleted mantle reservoir has a linear isotopic growth from  $^{176}\text{Hf}/^{177}\text{Hf} = 0.279718$  at 4.55 Ga to  $^{176}\text{Hf}/^{177}\text{Hf} = 0.283250$  at present, with  $^{176}\text{Lu}/^{177}\text{Hf}$  ratio of 0.0384 (Griffin *et al.* 2000). Two-stage model ages ( $T_{\text{DM2}}$ ) were also calculated, assuming that the parental magma was produced from an average continental crust ( $^{176}\text{Lu}/^{177}\text{Hf} = 0.015$ ; Griffin *et al.* 2002).

### 3.c. Major and trace element analyses

The samples were crushed and ground to 200 mesh. Whole-rock major and trace element analyses were obtained at ALS Chemex Co., Ltd (Guangzhou, China) using X-ray fluorescence spectrometer (XRF), ICP-MS and inductively coupled plasma-atomic emission spectrometry (ICP-AES). Details of the analytical procedure can be found in Zhou *et al.* (2002) and Liu *et al.* (2008). One pulp sample was fused with lithium metaborate–lithium tetraborate flux, including an oxidizing agent (lithium nitrate), and then poured into a platinum mold. The resultant disc was then analysed by XRF spectrometry. The XRF analysis was determined in conjunction with a loss-on-ignition at 1000 °C. The resulting data from both analyses were combined to produce a ‘total’. One prepared sample was added to lithium metaborate/lithium tetraborate flux, mixed well and fused in a furnace at 1025 °C. The resulting melt was then dissolved and cooled in an acid

mixture containing nitric, hydrochloric and hydrofluoric acids. This solution was then analysed by ICP-MS. Another prepared sample was digested with perchloric, nitric and hydrofluoric acids. The residue was leached with dilute hydrochloric acid and diluted to volume. The solution was then analysed using ICP-MS for ultratrace level elements. The same solution was also analysed using ICP-AES for trace level elements. Results were corrected for spectral inter-element interferences. The analytical accuracy and precision for the trace elements and major elements were found to be better than 5% and 10%, respectively.

## 4. Results

The U–Pb zircon isotopic data are listed in Supplementary Table 1, the Lu–Hf isotopic analyses in Supplementary Table 2 and major and trace element data are presented in Supplementary Table 3.

### 4.a. Zircon U–Pb ages

#### 4.a.1. Gabbro

Zircon grains are euhedral and stubby, 50–100 × 100–200 μm in size and exhibit concentric oscillatory zoning (Fig. 4). Except for the older spot 9, 22 concordant spots for sample 19DZH-17-2 yield a weighted mean  $^{206}\text{Pb}/^{238}\text{U}$  age of  $286.2 \pm 0.96$  Ma (MSWD = 0.62, Th/U = 0.52–1.07; Fig. 5a).

#### 4.a.2. Diorite

Zircon from the investigated diorite is all euhedral, prismatic and stubby. They have well-preserved oscillatory zoning and 30–80 × 60–180 μm in size (Fig. 4). Twenty-three spots were analysed for sample HBH2019-131-1, except for 6 older and younger spots,

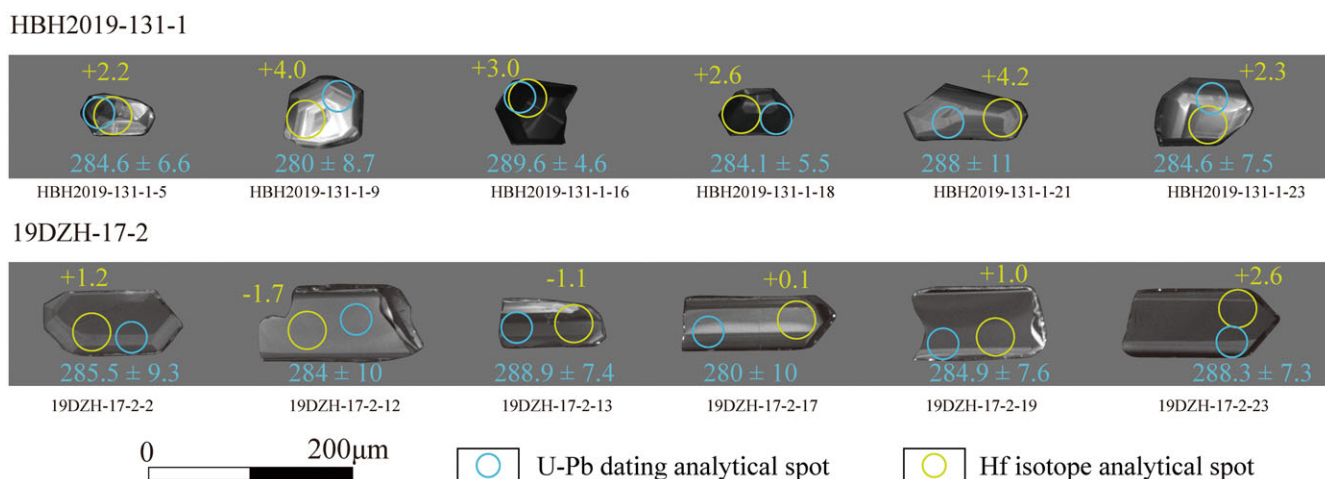


**Figure 4.** (Colour online) Cathodoluminescence (CL) images of representative zircons from studied gabbro and diorites. The blue line circle represents the spot of LA-ICP-MS analysis for U-Pb dating. The yellow line circle represents the spot of LA-MC-ICP-MS analysis for Lu-Hf isotope compositions. Apparent ages (in blue) and  $\epsilon_{\text{Hf}}(t)$  values (in yellow) are denoted.

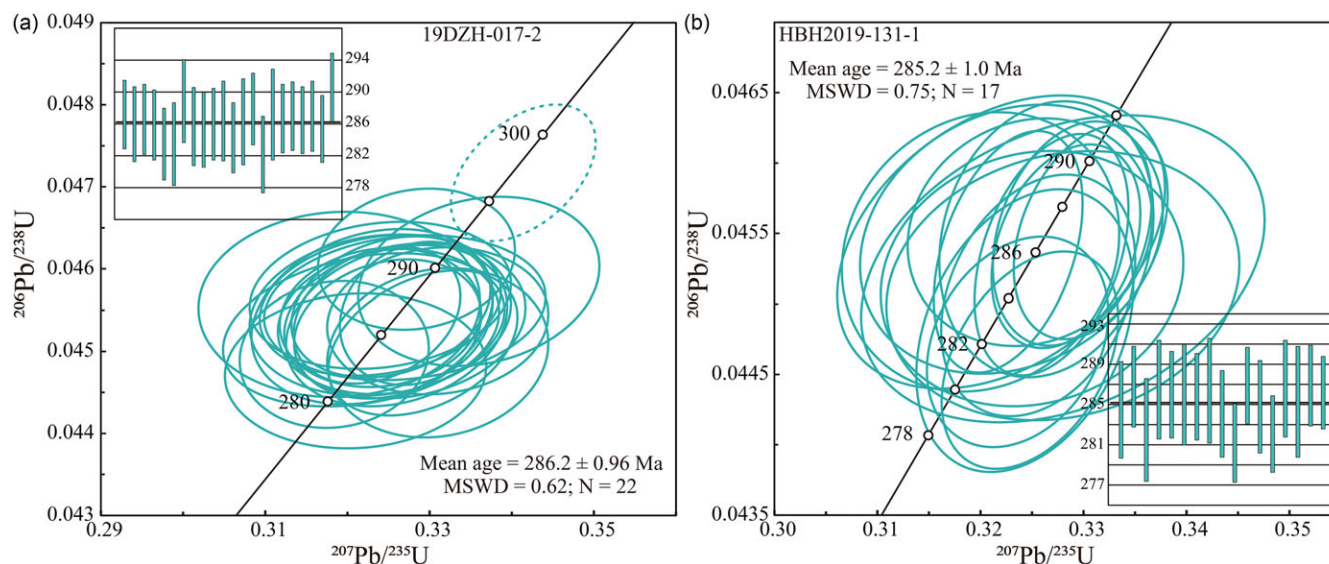


**Figure 5.** (Colour online) Concordia diagrams of LA-ICP-MS zircon U-Pb data from investigated gabbro and diorites in the Zhushileng-Hangwula Belt.

17 concordant spots yield a weighted mean  $^{206}\text{Pb}/^{238}\text{U}$  age of  $285.2 \pm 1.0$  Ma (MSWD = 0.75; Fig. 5b), with Th/U ratios of 0.52–1.55.

#### 4.b. Zircon Hf isotopic compositions

Twenty zircon grains from sample 19DZH-17-2 have variable  $\epsilon_{\text{Hf}}(t)$  values between  $-2.5$  and  $+2.6$  (Fig. 6), two-stage model ages ( $T_{\text{DM2}}$ ) of 1.96–1.49 Ma and initial  $^{176}\text{Hf}/^{177}\text{Hf}$  ratios of 0.282908–0.282971. Seventeen zircons from sample HBH2019-131-1 yield positive  $\epsilon_{\text{Hf}}(t)$  values between  $+1.2$  and  $+4.9$  (Fig. 6), two-stage model ages ( $T_{\text{DM2}}$ ) of 1.62–1.29 Ga and initial  $^{176}\text{Hf}/^{177}\text{Hf}$  ratios of 0.282627–0.282733.

#### 4.c. Whole-rock major and trace elements

The gabbro sample exhibits low contents of  $\text{SiO}_2$  (49.36 wt%) and  $\text{K}_2\text{O}$  (0.52 wt%), and high contents of  $\text{Fe}_2\text{O}_3^{\text{T}}$  (7.98 wt%),

$\text{CaO}$  (12.45 wt%) and  $\text{Mg}^\#$  [ $67.49$ ,  $\text{Mg}^\# = \text{Mg}/(\text{Mg} + \text{Fe}^{2+})$ ], which place the gabbro in the metaluminous field in the A/CNK [(molecular ratio of  $\text{Al}_2\text{O}_3/(\text{CaO} + \text{Na}_2\text{O} + \text{K}_2\text{O})$ ] versus A/NK [(molecular ratio of  $\text{Al}_2\text{O}_3/(\text{Na}_2\text{O} + \text{K}_2\text{O})$ ] diagram (Fig. 7b; Frost *et al.* 2001). The gabbro is transitional between calc-alkaline and tholeiitic (Fig. 7c) and exhibits total rare-earth elements (REEs) concentrations of 61.94 and slightly enriched light rare-earth elements (LREEs) [(La/Yb)<sub>N</sub> = 1.18], with almost no Eu anomalies [ $\delta\text{Eu} = 1.05$ ,  $\delta\text{Eu} = \text{EuN}/(\text{EuN} \times \text{GdN})^{1/2}$ ] (Fig. 8a). The gabbro exhibits enrichments in Rb, U and Sr, and depletions in Nb, Ta and Zr (Fig. 8d).

The diorites have low  $\text{SiO}_2$  (51.40–56.54 wt%), high  $\text{Al}_2\text{O}_3$  (15.02–18.42 wt%),  $\text{MgO}$  (3.46–6.42 wt%),  $\text{Mg}^\#$  (49.37–58.33) and  $\text{Fe}_2\text{O}_3^{\text{T}}$  (7.03–10.55 wt%), as well as low  $\text{K}_2\text{O} + \text{Na}_2\text{O}$  (3.87–4.33 wt%). They are metaluminous (A/CNK = 0.66–0.94; Fig. 7b) and belong to the tholeiitic to high calc-alkaline series (Fig. 7c). These diorites have total REE concentrations of



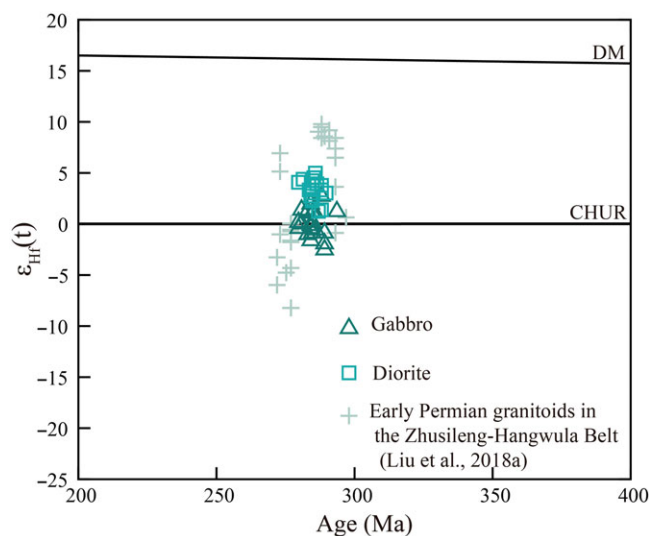


**Figure 6.** (Colour online) Zircon Hf isotopic compositions of the early Permian gabbro and diorites from the Zhusileng-Hangwula Belt. The  $\epsilon_{\text{Hf}}(t)$  values of the early Permian granitoids are from Liu *et al.* (2018a).

47.75–88.75 and enrichments in LREEs [(La/Yb)<sub>N</sub> = 3.44–6.37], with almost no Eu anomalies ( $\delta\text{Eu} = 0.71\text{--}1.02$ ) (Fig. 8a). Furthermore, they show enrichments in Rb, U, Pb and Sr, and depletions in Nb and Ta (Fig. 8b).

## 5. Discussion

The weighted mean  $^{206}\text{Pb}/^{238}\text{U}$  ages of  $286.2 \pm 0.96$  Ma and  $285.2 \pm 1.0$  Ma are interpreted as crystallization ages of gabbro and diorite, respectively.

### 5.a. Petrogenesis

#### 5.a.1. Gabbro

The early Permian gabbro in the Zhusileng-Hangwula Belt yielded variable zircon  $\epsilon_{\text{Hf}}(t)$  values (−2.5 to +2.6) and old  $T_{\text{DM}2}$  ages (1.96–1.49 Ga, average 1.68 Ga). The heterogeneous zircon  $\epsilon_{\text{Hf}}(t)$  values can be attributed either to melts derived from an asthenospheric mantle with crustal contamination or to those from an enriched lithospheric mantle (Wu *et al.* 2007). The gabbro sample exhibits high Al, Ca and Fe, and low Si, K and P, indicating a parental mantle source instead of crustal materials (e.g., Rundick & Gao, 2003). Furthermore, the content of  $\text{Mg}^\#$  (67.49) of this gabbro is close to the primary mantle-derived magma ( $\text{Mg}^\# = 68\text{--}73$ , Hess & Wiebe, 1989), ruling out crustal assimilation by primary mantle-derived magma. Therefore, we suggest that the Huisentala gabbro was likely derived from an enriched lithospheric mantle.

On the chondrite-normalized REE diagram (Fig. 8a), the gabbros are characterized by enrichments in LREEs. As shown in the primitive mantle-normalized trace-element spider diagram (Fig. 8b), the gabbro is characterized by relative enrichment in large ion lithophile elements (LILEs) and U, and depletion in high field strength elements (HFSEs) (e.g., Ti, Nb and Ta), indicative of arc geochemical affinities. Crustal contamination or magma source metasomatization by subduction-related materials may result in the negative Nb–Ta–Ti anomalies (Sun & McDonough, 1989; Chen *et al.* 2011; Tang *et al.* 2014; Xia, 2014). However, crustal contamination can be

ruled out in the generations of the Huisentala gabbro due to its high content of  $\text{Mg}^\#$ . Moreover, the gabbro displays high Ba/Th ratio (43.73) and relatively low Hf/Sm ratio (0.73), indicating the contribution of subduction-related fluids in its generations (La Flèche Camire & Genner, 1998; Pearce & Stern, 2006). Xia *et al.* (2007) suggested that magmatic rocks influenced by subduction fluids/melts usually present low Zr contents (<130 ppm) and Zr/Y ratios (<4). The Huisentala gabbro has low content of Zr (64 ppm) and Zr/Y ratio (3.66). Therefore, we proposed that the Huisentala gabbro was derived from an enriched lithospheric mantle metasomatized by subduction-related fluids.

#### 5.a.2. Diorite

The Huodonghaer diorites have high MgO (3.46–6.32 wt%), Cr (average 73.33 ppm) and Ni (average 23.10 ppm), as well as low  $\text{FeO}^\text{T}/\text{MgO}$  (1.27–1.83) ratios,  $\text{TiO}_2$  (0.48–0.90 wt%) and (La/Yb)<sub>N</sub> (3.44–6.37) ratios, indicating high-Mg andesite compositions (Kelemen *et al.* 2003; Tatsumi, 2006; Zhao *et al.* 2009). The Huodonghaer diorites have a higher  $\text{Mg}^\#$  range (49.37–58.33) than pure crustal melts (Patiño Douce & Beard, 1995; Rundick & Gao, 2003), so they most likely formed from mantle melts that were influenced by crustal materials rather than from a crustal source (Jiang *et al.* 2009; Dong *et al.* 2012).

Partial melting of mantle peridotite that is metasomatized by the slab melts or subducted sediment-related melts has been regarded as the most likely petrogenetic model for high-Mg diorite (Martin *et al.* 2005; Moyaen, 2009; Dong *et al.* 2012). High-Mg diorite derived from the reaction between mantle peridotite and slab melts usually exhibits adakite-like geochemical characteristics, such as high  $\epsilon_{\text{Nd}}(t)$  values, high Sr contents, low Y and Yb contents, high Sr/Y and (La/Yb)<sub>N</sub> ratios (Yin *et al.* 2015). However, the Huodonghaer diorites display positive zircon  $\epsilon_{\text{Hf}}(t)$  values (+1.2 to +4.9), high Y (13.20–19.30) and Yb (1.41–2.07), and low Sr/Y (21.14–45.61) and (La/Yb)<sub>N</sub> ratios (3.44–6.37). In addition, they have consistently low U/Th (0.12–0.33) and high Th/Nb (0.37–0.77) ratios, similar to the marine sediments (Fig. 9a). Furthermore, the Huodonghaer diorites have high and variable Th/Yb ratios, inconsistent with Ba/La ratios, which also support the involvement of a sediment-derived melts rather than of slab-derived fluids (Tatsumi, 2006; Fig. 9b). Because Ba is more soluble in aqueous fluids than La (Hanyu *et al.* 2006), the Ba/Th ratios should be markedly increased if oceanic crust-derived melts are involved in the production of magmas. Therefore, we suggest that the Huodonghaer diorites were derived from the partial melting of mantle peridotite that was metasomatized by the subducted sediment-derived melts.

#### 5.b. Tectonic implications

The Zhusileng-Hangwula Belt, located in the southernmost segment of the CAOB, is a pivotal region for determining the tectonic evolutionary history of the PAO. The Zhusileng-Hangwula Belt experienced multiple magmatic activities from the end of the early Palaeozoic to the late Palaeozoic, including four stages of ca. 399–373, 325–310, 296–263 and 250–216 Ma (Dang *et al.* 2011; Liu *et al.* 2018a, b; Shi *et al.* 2018; Chen *et al.* 2019; Fei *et al.* 2019; Li, 2020; Song *et al.* 2020; Zhao *et al.* 2020). However, as we mentioned in the introduction, the tectonic setting of the northern Alxa Block during the late Carboniferous–Permian is still ambiguous.

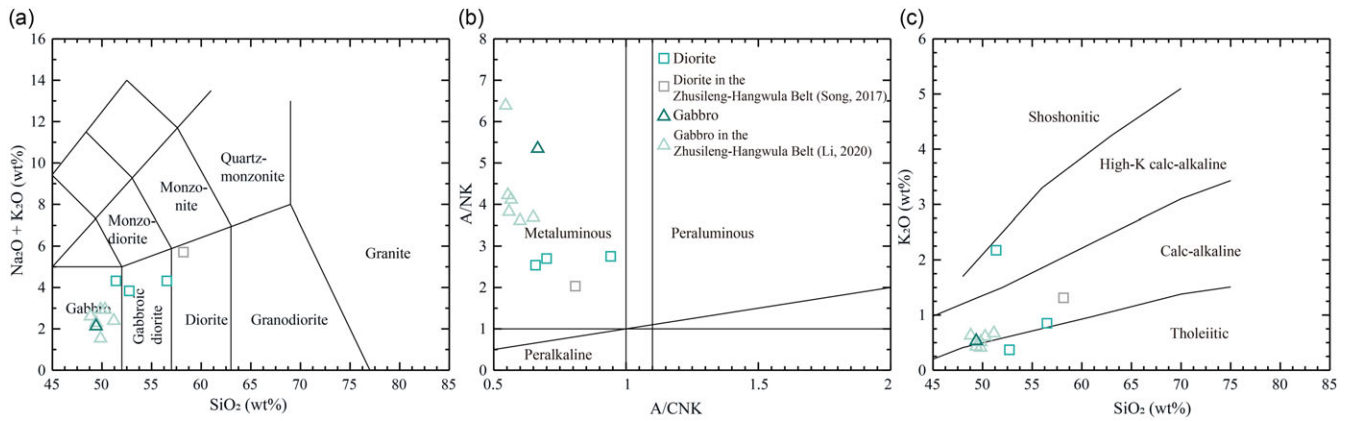


Figure 7. (Colour online) Diagrams showing major element features of the studied gabbro and diorites.

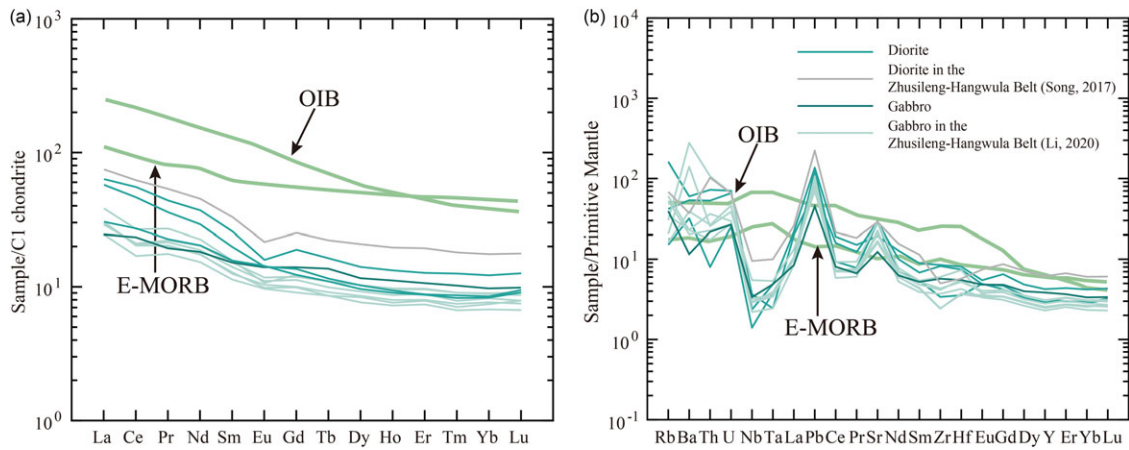


Figure 8. (Colour online) (a) Chondrite-normalized rare earth element patterns and (b) primitive mantle-normalized trace element spider diagrams for the investigated gabbro and diorites from the Zhushileng-Hangwula Belt. Compositions of chondrite and primitive mantle refer to Sun and McDonough (1989).

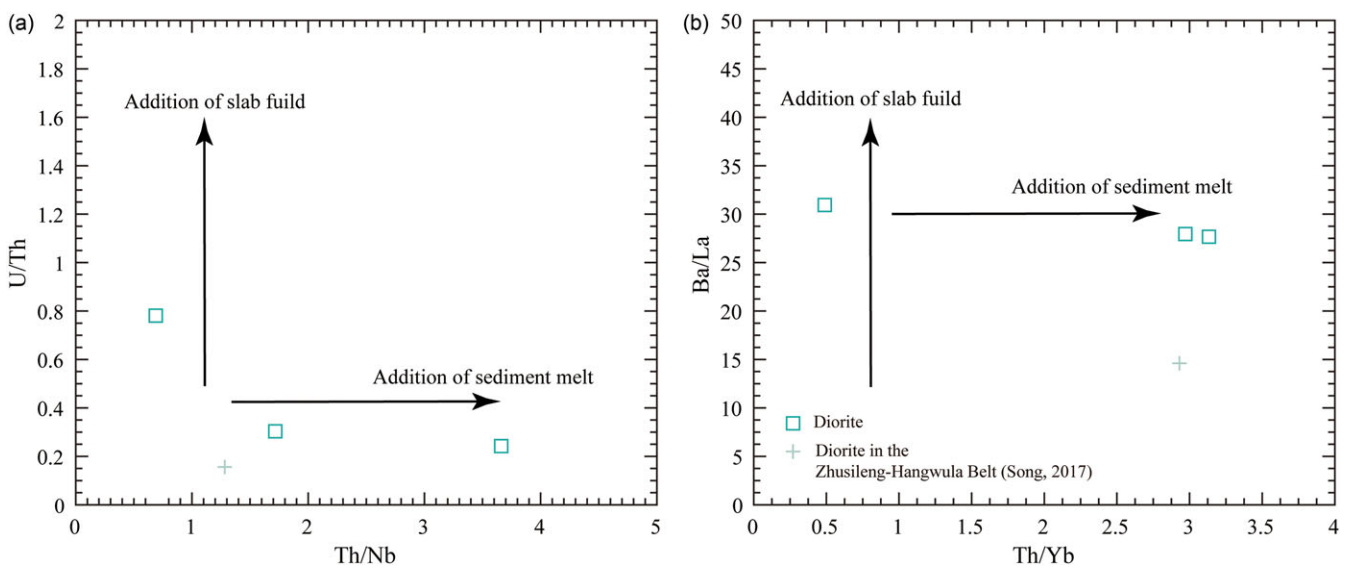
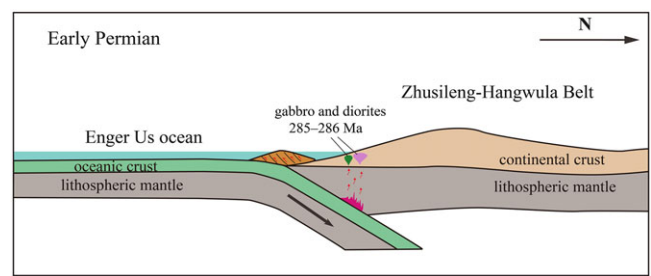


Figure 9. (Colour online) (a) Th/Nb versus U/Th and (b) Th/Yb versus Ba/La discrimination diagrams (modified after Tatsumi, 2006 and Hanyu et al. 2006).

Fei *et al.* (2019) proposed that the late Carboniferous to early Permian intrusions in the Zhusileng–Hangwula Belt formed in a post-collision setting, which indicates that the PAO had closed before the early Permian (Li *et al.* 2020), and then evolved into an extensional setting to form a rift along the north Alxa Block. However, the Palaeozoic strata in the Zhusileng area formed an NW–SE-trending anticline, which was intruded by late Palaeozoic granite (Zhang *et al.* 2022). The youngest strata involved in this fold are early Permian, and they are unconformably covered by late Permian strata (Liu *et al.* 2019). The formation of this anticline reflected horizontal compression that occurred during the early to late Permian, probably as a result from the closure of the PAO. The report of radiolarians fossil (Xie *et al.* 2014) and late Carboniferous normal mid-ocean ridge basalts exposed in the Enger Us ophiolite (~302 Ma, Zheng *et al.* 2014) imply that the PAO still existed during the late Carboniferous–early Permian. Liu *et al.* (2017) suggested that a switch of the tectonic settings, which was attributed to the final closure of the PAO, occurred at 280–265 Ma, according to the marked shift of zircon  $\epsilon_{\text{Hf}}(t)$  values and whole-rock  $\epsilon_{\text{Nd}}(t)$  values of the granitoids from the northern Alxa Block. Therefore, a post-collisional setting is not consistent with the derivation of the early Permian intrusions from the Zhusileng–Hangwula Belt.

The gabbro exhibits enrichment in LREE and U, and depletion in HFSE (e.g., Ti, Nb and Ta), indicative of arc-like geochemical affinities (Fig. 8), and we suggest that the gabbro was derived from an enriched lithospheric mantle metasomatized by subduction-related fluids. Furthermore, we identified that almost coeval high-Mg diorites occur in the Zhusileng–Hangwula Belt. High-Mg diorites are generally related to the subduction of a young and/or hot oceanic slab (e.g., ridge subduction) (Rogers & Saunders, 1989; Furukawa & Tatsumi, 1999). Sedimentological and palaeocurrents analyses on early Permian strata in the Zhusileng area also supported a subduction setting (Chen *et al.* 2011; Jiang *et al.* 2012; Shi *et al.* 2013; Zhang *et al.* 2022). Moreover, Li (2020) proposed that the gabbros in the Yagan metamorphic core complex have been strongly deformed and formed dykes, most of which are cut by normal faults resulting from the extensional deformation of the crust in this region. That implies that the formation of the gabbro was prior to the extensional event occurring after the closure of the PAO. Furthermore, coeval granitoid displaying volcanic arc affinities have also been verified in the Zhusileng–Hangwula Belt (Li *et al.* 2020; Song *et al.* 2020; Zhao *et al.* 2020; Deng *et al.* 2022b). For instance, the 298–290 Ma granitoids in the Zhusileng–Hangwula Belt were generated by magma mixing and formed in a subduction setting (Liu *et al.* 2018a). Therefore, we propose that the early Permian gabbro and coeval high-Mg diorites in the Zhusileng–Hangwula Belt are formed in an ocean slab subduction environment (Fig. 10).

We believe that the PAO in the middle part of the southern CAOB closed during the middle-late Permian for the following reasons: (1) middle-late Permian A-type and bimodal volcanic rocks found in this unit (Song *et al.* 2018, 2019, 2020; Li, 2019) indicate a post-collisional tectonic setting in the Zhusileng–Hangwula Belt after the early Permian; (2) late Permian sandstones (256–254 Ma) are interpreted to have formed in a post-collision setting, as suggested by geochemical characteristics (Liu *et al.* 2019; Shi *et al.* 2020) and (3) heavy mineral features of the Permian strata in Zhusileng and adjacent areas reveal that the detritus was sourced from both the northern and southern Alxa Block, which support that the PAO closed between the early and late Permian (Chen *et al.* 2019; Zhang *et al.* 2022). Thus, the Zhusileng–Hangwula Belt



**Figure 10.** (Colour online) Schematic cartoon showing the early Permian tectonic model of the Zhusileng–Hangwula Belt.

was an ocean subduction setting during the early Permian, then transitioned from subduction to collision and then to post-collision in the middle-late Permian probably due to the closure of the PAO along the Enger Us suture.

## 6. Conclusions

Based on the geochronological, geochemical and zircon Hf isotopic data for the gabbro and diorites in the Zhusileng–Hangwula Belt and previous studies, the following conclusions can be drawn:

- (1) Zircon LA-ICP MS U–Pb age data show that the monzogranites, Huisentala gabbro and Huodonghaer diorites from the Zhusileng–Hangwula Belt were formed during the early Permian (291–285 Ma).
- (2) The Huisentala gabbro yielded variable zircon  $\epsilon_{\text{Hf}}(t)$  values (–2.5 to +2.6) and old  $T_{\text{DM}2}$  ages (1.96–1.49 Ga, average 1.68 Ga). The gabbro sample exhibits high Al, Ca, Fe, Mg<sup>#</sup> and LREE, and low Si, K, P and HFSE, with slightly negative Eu anomalies, and was likely derived from an enriched lithospheric mantle metasomatized by subduction-related fluids. The Huodonghaer diorites exhibit high-Mg diorite-like geochemical compositions, such as high MgO, Sr and Cr contents, and low FeO/MgO ratios. They show moderate zircon  $\epsilon_{\text{Hf}}(t)$  values (+1.2 to +4.9) and Mesoproterozoic two-stage model ages (1.62–1.29 Ga), indicating that the diorites are derived from partial melting of mantle peridotite that was metasomatized the subducted sediment-derived melts.
- (3) Combined with other geological evidence, we propose that the early Permian gabbro and coeval high-Mg diorites from the Zhusileng–Hangwula Belt formed in an ocean subduction setting and probably are associated with the tectonic evolution of the PAO along the Enger Us suture.

**Supplementary material.** The supplementary material for this article can be found at <https://doi.org/10.1017/S0016756823000444>

**Data availability statement.** The data that support the findings of this study are available in the supplementary material of this article.

**Acknowledgements.** This work was financially supported by the China Geological Survey (DD20221768, DD20190011, DD20221643). We are grateful to anonymous reviewers for their constructive comments. We are also grateful to Liming Zhou (National Research Center for Geoanalysis, Chinese Academic of Science, Beijing) for his help in zircon Lu–Hf isotopic analysis, Dr. Zengzheng Wang for reviewing the manuscript and offering valuable advice, Dr. Shenglin Xu for helpful discussions in U–Pb geochronological analysis and Dr. Yongchao Wang, Wei Yu, He Su, Yiping Zhang and Bing Li for assistance in our field work.



**Competing interests.** The authors declare that they have no known competing financial interests or personal relationships that could have appeared to influence the work reported in this paper.

## References

- BGMRIM (Bureau of Geology and Mineral Resources of Inner Mongolia Autonomous Region)** (1991) *Regional Geology of Inner Mongolia Autonomous Region*. Beijing: Geological Publishing House, 725 pp (in Chinese).
- Bouvier A, Vervoort JD and Patchett PJ** (2008) The Lu–Hf and Sm–Nd isotopic composition of CHUR: constraints from unequilibrated chondrites and implications for the bulk composition of terrestrial planets. *Earth and Planetary Science Letters* **273**, 48–57.
- Chen GC, Li YH, Shi JZ, Li JC and Zhao SL** (2011) Heavy mineral characteristics of Carboniferous–Permian strata in Ejin Banner and its vicinities, western Inner Mongolia, and their significance. *Geological Bulletin China* **30**, 962–71 (in Chinese with English abstract).
- Chen XJ, Shu LS and Santosh M** (2011) Late Paleozoic post-collisional magmatism in the Eastern Tianshan Belt, Northwest China: new insights from geochemistry, geochronology and petrology of bimodal volcanic rocks. *Lithos* **127**, 581–98.
- Chen Y** (2015) Variscan Granite Magmatism in Guaizihu Area of Ejinaqi, Inner Mongolia, China. Diploma thesis, Chang’ an University, Xi’ an, China. Published thesis (in Chinese with English abstract).
- Chen Y, Wu TR, Gan LS, Zhang ZC and Fu B** (2019) Provenance of the early to mid-Paleozoic sediments in the northern Alxa area: implications for tectonic evolution of the southwestern Central Asian Orogenic Belt. *Gondwana Research* **67**, 115–30.
- Dang B, Zhao H, Lin GC, Wu KL, Kang XY, Ge HY, Wu B and Liu SH** (2011) Geochemistry and tectonic setting of Permian volcanic rocks in Yingen–Ejin Banner basin and its neighboring areas, western Inner Mongolia. *Geological Bulletin of China* **30**, 923–31 (in Chinese with English abstract).
- Deng WB, Shao ZG, Wang ZZ, Chen XH, Yi JJ and Xu HJ** (2022b) Geochemistry and zircon U–Pb–Hf isotopes of granodiorites in the northern Alxa area: implications for the Middle–Late Devonian tectonic evolution of the southern Central Asian Orogenic Belt. *International Journal of Earth Sciences* **111**, 2369–90.
- Deng WB, Shao ZG, Xu HJ and Chen XH** (2023) Late Palaeozoic tectonic evolution of the southern Central Asian Orogenic Belt: constraints from the Early Permian magmatism in the northern Alxa area. *Geological Journal* **58**, 1–16.
- Deng WB, Shao ZG, Xu HJ, Yi JJ, Xu DX and Zhang SJ** (2022a) Tectonic affinity of the Zhusileng–Hangwula Belt in the northern Alxa area: evidence from the zircon U–Pb ages and Hf isotopic compositions of the Mesoproterozoic (~1.4 Ga) igneous rocks. *Geological Journal* **57**, 4451–73.
- Dong YP, Liu XM, Zhang GW, Chen Q, Zhang XN, Li W and Yang C** (2012) Triassic diorites and granitoids in the Foping area, constraints on the conversion from subduction to collision in the Qinling orogen, China. *Journal of Asian Earth Sciences* **47**, 123–42.
- Eizenhöfer PR, Zhao G, Zhang J and Sun M** (2014) Final closure of the Paleo-Asian Ocean along the Solonker suture zone: constraints from geochronological and geochemical data of Permian volcanic and sedimentary rocks. *Tectonics* **33**, 441–63.
- Fei MM, Pan M, Xie CL, Wang JH and Zhao HS** (2019) Timing and tectonic settings of the Late Paleozoic intrusions in the Zhusileng, northern Alxa, implication for the metallogeny. *Geosciences Journal* **23**, 39–57.
- Frost BR, Barners CG, Collins WJ, Arculus RJ, Ellis DJ and Frost CD** (2001) A geochemical classification for granitic rocks. *Journal of Petrology* **42**, 2033–48.
- Furukawa Y and Tatsumi Y** (1999) Melting of a subducting slab and production of high-Mg andesite magmas: unusual magmatism in SW Japan at 13–15 Ma. *Geophysical Research Letters* **26**, 2271–4.
- Geng YS and Zhou XW** (2012) Early Permian magmatic events in the Alxa metamorphic basement, evidence from geochronology. *Acta Petrologica Sinica* **28**, 2667–85 (in Chinese with English abstract).
- Griffin WL, Pearson NJ, Belousova E, Jackson SE, Van Achterberg E, O’Reilly SY and Shee SR** (2000) The Hf isotope composition of cratonic mantle: LAM-MC-ICPMS analysis of zircon megacrysts in kimberlites. *Geochimica et Cosmochimica Acta* **64**, 133–47.
- Griffin WL, Wang X, Jackson SE, Pearson NJ, O’Reilly SY, Xu XS and Zhou XM** (2002) Zircon geochemistry and magma mixing, SE China: in-situ analysis of Hf isotopes, Tonglu and Pingtan igneous complexes. *Lithos* **61**, 237–69.
- Han BF, Zhang C, Zhao L, Xu Z, Chen JF, Zhang L, Zhou YZ and Song B** (2010) A preliminary study of granitoids in western Inner Mongolia. *Acta Petrologica Et Mineralogica* **29**, 741–49 (in Chinese with English abstract). <http://doi.org/10.3724/SP.J.1084.2010.00199>
- Hanyu T, Tatsumi Y, Nakai SI, Chang Q, Miyazaki T, Sato K, Tani K, Shibata T and Yoshida T** (2006) Contribution of slab melting and slab dehydration to magmatism in the NE Japan arc for the last 25 Myr: constraints from geochemistry. *Geochemistry Geophysics Geosystems* **7**, Q08002.
- Hess PC and Wiebe RA** (1989) *Origins of Igneous Rocks*. London: Harvard University Press, 279 pp.
- Hong DW, Zhang JS, Wang T, Wang SG and Xie XL** (2004) Continental crustal growth and the supercontinental cycle: evidence from the Central Asian Orogenic Belt. *Journal of Asian Earth Sciences* **23**, 799–813.
- Hou KJ, Li YH, Zou TR, Qu XM, Shi YR and Xie GQ** (2007) Laser ablation-MC-ICPMS technique for Hf isotope microanalysis of zircon and its geological applications. *Acta Petrologica Sinica* **23**, 2595–3604 (in Chinese with English abstract).
- Jackson SE, Pearson NJ, Griffin WL and Belousova EA** (2004) The application of laser ablation-inductively coupled plasma-mass spectrometry to in situ U–Pb zircon geochronology. *Chemical Geology* **211**, 47–69.
- Jahn BM, Windley BF, Natal’in B and Dobretsov N** (2004) Phanerozoic continental growth in Central Asia. *Journal of Asian Earth Sciences* **23**, 599–603.
- Jiang T, Han W, Shi JZ, Chen GC, Wei JS and Zhang HY** (2012) The application of heavy minerals to analyzing sediment provenance: a case study of the Carboniferous–Permian strata in Ejin Banner and its adjacent areas. *Geological Bulletin China* **31**, 1692–702 (in Chinese with English abstract).
- Jiang YH, Jiang SY, Dai BZ, Liao SY, Zhao KD and Ling HF** (2009) Middle to Late Jurassic felsic and mafic magmatism in southern Hunan Province, Southeast China: implications for a continental arc to rifting. *Lithos* **107**, 185–204.
- Kelemen PB, Hanghøj K and Greene AR** (2003) One view of the geochemistry of subduction-related magmatic arcs, with an emphasis on primitive andesite and lower crust. *Treatise on Geochemistry* **3**, 1–70.
- La Flèche MR, Camire G and Jenner GA** (1998) Geochemistry of post-Acadian, Carboniferous continental intraplate basalts from the Maritimes Basin, Magdalen islands, Quebec, Canada. *Chemical Geology* **148**, 115–36.
- Li JJ** (2006) Regional metallogenic system of Alashan Block in Inner Mongolia autonomous region, China. PhD thesis. China University of Geosciences (Beijing), Beijing, China. Published thesis (in Chinese with English abstract).
- Li RW** (2020) Geochemistry and tectonic implications of gabbros and granites in the northern Alxa, NW China. Diploma thesis, Lanzhou University, Lanzhou, China. Published thesis (in Chinese with English abstract).
- Li RW, Zhang X, Shi Q, Chen WF, An Y, Huang YS, Liu YX and Wang JR** (2020) Geochemistry and Nd–Hf isotopes of the Early Permian volcanic rocks in Hangwula of northern Alxa area and their tectonic significance. *Geological Bulletin of China* **39**, 647–58 (in Chinese with English abstract).
- Li YQ** (2019) Geochemistry of Volcanic Rocks in the Jinta Formation of North to Alxa Block and Its Tectonic Implications. Diploma thesis, Lanzhou University, China. Published thesis (in Chinese with English abstract).
- Liu Q, Zhao GC, Han YG, Eizenhöfer PR, Zhu YL, Hou WZ, Zhang XR and Wang B** (2017) Timing of the final closure of the Paleo-Asian Ocean in the Alxa terrane: constraints from geochronology and geochemistry of Late Carboniferous to Permian gabbros and diorites. *Lithos* **274–275**, 19–30.
- Liu Q, Zhao GC, Han YG, Li XP, Zhu YL, Eizenhöfer PR, Zhang XR, Wang B and Tsui RW** (2018a) Geochronology and geochemistry of Paleozoic to Mesozoic Granitoids in Western Inner Mongolia, China: implications for the tectonic evolution of the Southern Central Asian Orogenic Belt. *The Journal of Geology* **126**, 451–71.

- Liu Q, Zhao GC, Han YG and Zhu YL (2018b) Timing of the final closure of the middle segment of the Paleo-Asian Ocean, insights from geochronology and geochemistry of Carboniferous–Triassic volcano-sedimentary successions in western Inner Mongolia, China. *Geological Society of America Bulletin* **131**, 941–65.
- Liu Q, Zhao GC, Han YG, Zhu YL, Wang B., Eizenhöfer PR, Zhang XR and Tsui RW (2019) Timing of the final closure of the middle segment of the Paleo-Asian Ocean: insights from geochronology and geochemistry of Carboniferous–Triassic volcanosedimentary successions in western Inner Mongolia, China. *Geological Society of America Bulletin* **131**, 941–65.
- Liu YS, Zong KQ, Kelemen PB and Gao S (2008) Geochemistry and magmatic history of eclogites and ultramafic rocks from the Chinese continental scientific drill hole: subduction and ultrahigh-pressure metamorphism of lower crustal cumulates. *Chemical Geology* **247**, 133–53.
- Ludwig KR (2003) *ISOPLOT 3.00: A Geochronological Toolkit for Microsoft Excel*. Berkeley, CA: Berkeley Geochronology Center, 39 pp.
- Martin H, Smithies RH, Rapp R, Moyen JF and Champion D (2005) An overview of adakite, tonalite–trondhjemite–granodiorite (TTG), and sanukitoid, relationships and some implications for crustal evolution. *Lithos* **79**, 1–24.
- Moyen JF (2009) High Sr/Y and La/Yb ratios: the meaning of the “adakitic signature”. *Lithos* **112**, 556–74.
- Patino Douce AE and Beard JS (1995) Dehydration–melting of biotite and quartz amphibolite from 3 to 15 kb. *Journal of Petrology* **36**, 707–38.
- Pearce JA and Stern RJ (2006) Origin of back-arc basin magmas: trace element and isotope perspectives. In *Back Arc Spreading Systems: Geological, Biological, Chemical, and Physical Interactions* (eds DM Christie, CR Fisher, SM Lee and S Givens), pp. 63–86. American Geophysical Union, Geophysical Monograph Series 166.
- Qing Y (2010) Study of the Metamorphosed basement in Tamusu region of Alxa Youqi, Inner Mongolia. Diploma thesis, Chang’an University, Xi’an, China. Published thesis (in Chinese with English abstract).
- Rogers G and Saunders AD (1989) Magnesian andesites from Mexico, Chile and the Aleutian Islands: implications for magmatism associated with ridge-trench collision. In *Boninites and Related Rocks* (ed AJ Crawford), p. 445. London: Unwin Hyman.
- Rundick RL and Gao S (2003) Composition of the continental crust. In *Treatise on Geochemistry* (eds DH Heinrich & KK Turekian), p. 64. Oxford: Elsevier-Pergamon.
- Scherer EE, Whitehouse MJ and Muenker C (2007) Zircon as a monitor of crustal growth. *Elements* **3**, 19–24.
- Şengör AC, Natalin BA and Burtman VS (1993) Evolution of the Alaid tectonic collage and Palaeozoic crustal growth in Eurasia. *Nature* **364**, 299–306.
- Shi JZ, Chen GC, Jiang T, Niu YZ and Han W (2013) The provenance of Carboniferous Xiaodushanian–Permian Zisongian stage in Yingen–Ejin Banner Basin and its vicinities. *Geological Bulletin of China* **32**, 1777–89 (in Chinese with English abstract).
- Shi JZ, Lu JC, Wei JS, Niu YZ, Jiang T, Han XF and Xu W (2018) Petrology, geochemistry and sedimentary environment of Permian siliceous rocks in Yingen–Ejin basin and its adjacent areas. *Geological Bulletin of China* **37**, 120–31 (in Chinese with English abstract).
- Shi XJ, Wang T, Zhang L, Castro A, Xiao XC, Tong Y, Zhang JJ, Guo L and Yang QD (2014) Timing, petrogenesis and tectonic setting of the Late Paleozoic gabbro–granodiorite–granite intrusions in the Shalazhashan of northern Alxa, constraints on the southernmost boundary of the Central Asian Orogenic Belt. *Lithos* **208–209**, 158–77.
- Shi XJ, Zhang L, Wang T, Zhang JJ, Liu HM, Zhou HS and Yan YT (2016) Zircon geochronology and Hf isotopic compositions for the Mesoproterozoic gneisses in Zongnashan area, northern Alxa and its tectonic affinity. *Acta Petrologica Sinica* **32**, 3518–36 (in Chinese with English abstract).
- Shi XJ, Zhang L, Zhang CG, Zhang JJ, Ding ZY, Zhang Y, Bao JF and Zhou SH (2020) Zircon geochronology and geochemistry of the granitoids in Yagan area, northern Alxa and their tectonic implications. *Earth Science* **45**, 2469–2484. (in Chinese with English abstract).
- Song B, Zhang Y, Wan Y and Jian P (2002) Mount making and procedure of the SHRIMP dating. *Geographical Review* **48**, 26–30.
- Song DF, Xiao WJ, Collins AS, Glorie S, Han C and Li Y (2017) New chronological constrains on the tectonic affinity of the Alxa Block, NW China. *Precambrian Research* **299**, 230–43.
- Song DF, Xiao WJ, Collins AS, Glorie S, Han C and Li Y (2018) Final subduction processes of the PaleoAsian Ocean in the Alxa Tectonic Belt (NW China): constraints from field and chronological data of Permian arc-related volcano-sedimentary rocks. *Tectonics* **37**, 1658–87.
- Song DF, Xiao WJ, Collins AS, Glorie S, Han C and Li Y (2019) Late Carboniferous–early Permian arc magmatism in the south-western Alxa Tectonic Belt (NW China): constraints on the late Palaeozoic subduction history of the Palaeo-Asian Ocean. *Geological Journal* **54**, 1046–63.
- Song DF, Xiao WJ, Windley BF and Han CM (2020) Carboniferous to early Triassic magmatism and accretion in Alxa (NW China), Implications for accretionary orogenesis of the southern Altaids. *Journal of the Geological Society* **177**, 2020–46.
- Song W (2014) Research on Precambrian metamorphosed plutonic intrusions in the Northern Alxa, Inner Mongolia. Diploma thesis, China University of Geosciences (Beijing), Beijing, China. Published thesis (in Chinese with English abstract).
- Sun SS and McDonough WF (1989) Chemical and isotopic systematics of oceanic Basalts: implications for mantle composition and processes. *Geological Society, London Special Publications* **42**, 313–45.
- Tang GJ, Chung SL, Wang Q, Wyman DA, Dan W, Chen HY and Zhao ZH (2014) Petrogenesis of a Late Carboniferous mafic dike–granitoid association in the western Tianshan: response to the geodynamics of oceanic subduction. *Lithos* **202–203**, 85–9.
- Tatsumi Y (2006) High-Mg andesites in the Setouchi volcanic belt, southwestern Japan: analogy to Archean magmatism and continental crust formation? *Annual Review of Earth and Planetary Sciences* **34**, 467–99.
- Wang MM, Zhang L, Huo YJ, Shi XJ and Liu C (2019) Tectonic affinity of the northern Longshoushan–Beidashan: constraints from the zircon U–Pb age and Hf isotopic compositions of the Haisen Chulu gneiss. *Acta Petrologica ET Mineralogica* **38**, 631–645 (in Chinese with English Abstract).
- Wang T, Zheng YD, Gehrels GE and Mu ZG (2001) Geochronological evidence for existence of South Mongolian microcontinent: a zircon U–Pb age of granitoid gneisses from the Yagan–Onch Hayrhan metamorphic core complex. *Chinese Science Bulletin* **46**, 2005–8 (in Chinese with English Abstract).
- Wang T, Zheng YD, Liu SW, Li TB and Ma MB (2002) Mylonitic Potassic Granitoids from the Yagan metamorphic core complex on Sino-Mongolian border: a mark of transition from contractile to extensional tectonic regime. *Acta Petrologica Sinica* **18**, 177–86 (in Chinese with English Abstract).
- Wang ZZ, Han BF, Feng LX, Liu B, Zheng B and Kong LJ (2016) Tectonic attribution of the Langshan area in western Inner Mongolia and implications for the Neoproterozoic–Paleoproterozoic evolution of the western north china craton: evidence from LA-ICP-MS zircon U–Pb dating of the Langshan basement. *Lithos* **261**, 278–95.
- Wang ZZ, Han BF, Feng LX, Liu B, Zheng B, Kong LJ and Qi CY (2021) Early–middle Permian plutons in the Langshan area, western Inner Mongolia, China, and their tectonic implications. *Lithos* **382–383**, 105934.
- Wilhem C, Windley BF and Stampfli GM (2012) The Altaids of Central Asia: a tectonic and evolutionary innovative review. *Earth Science Review* **113**, 303–41.
- Windley BF, Dmitriy A, Xiao WJ, Kröner A and Badarch G (2007) Tectonic models for accretion of the Central Asian Orogenic Belt. *Bicentennial Review* **164**, 31–47.
- Wu FY, Jahn BM, Wilde SA, Lo CH, Yui TF, Lin Q, Ge WC and Sun DY (2003) Highly fractionated I-type granites in NE China (I): geochronology and petrogenesis. *Lithos* **66**, 241–73.
- Wu FY, Li XH, Zheng YF and Gao S (2007) Lu–Hf isotopic systematics and their applications in petrology. *Acta Petrologica Sinica* **23**, 185–220.
- Wu TR and He GQ (1993) Tectonic units and their fundamental characteristics on the northern margin of the Alxa block. *Acta Geologica Sinica* **6**, 373–85.
- Wu TR, He GQ and Zhang C (1998) On Paleozoic tectonics in the Alxa region. *Acta Geologica Sinica* **72**, 256–63 (in Chinese with English abstract).
- Xia LQ (2014) The geochemical criteria to distinguish continental basalts from arc related ones. *Earth Science Review* **139**, 195–212.



- Xia LQ, Xia ZC, Xu XY, Li XM and Ma ZP (2007) The discrimination between continental basalt and island arc basalt based on geochemical method. *Acta Petrologica et Mineralogica* **26**, 77–89.
- Xiao WJ, Windley BF, Allen MB and Han C (2013) Paleozoic multiple accretionary and collisional tectonics of the Chinese Tianshan orogenic collage. *Gondwana Research* **23**, 1316–41.
- Xiao WJ, Windley BF, Han C, Liu W, Wan B, Zhang JE, Ao S, Zhang Z and Song DF (2018) Late Paleozoic to early Triassic multiple roll-back and oroclinal bending of the Mongolia collage in Central Asia. *Earth Science Review* **186**, 94–128.
- Xie FQ, Wu JH, Sun YH, Wang LD, Wu JZ and Jia WJ (2021) Permian to Triassic tectonic evolution of the Alxa Tectonic Belt, NW China: constraints from petrogenesis and geochronology of felsic intrusions. *Lithos* **384–385**, 105980. <https://doi.org/10.1016/j.lithos.2021.105980>
- Xie L, Yin HQ, Zhou HR and Zhang WJ (2014) Permian radiolarians from the Engeerwusu suture zone in Alxa area of Inner Mongolia and its geological significance. *Geological Bulletin of China* **33**, 691–7 (in Chinese with English abstract).
- Xu B, Charvet J, Chen Y, Zhao P and Shi G (2013) Middle Paleozoic convergent orogenic belts in western Inner Mongolia (China): framework, kinematics, geochronology and implications for tectonic evolution of the Central Asian Orogenic Belt. *Gondwana Research* **23**, 1342–64.
- Yin HQ, Zhou HR, Cheng R, Zhang WJ, Zheng XM, Yang LY, Li J and Wang SY (2015) The Age, sedimentary characteristics and tectonic significance on the Yuanbaoshan formation in the southern margin of the Siberian plate, north of Alxa, Inner Mongolia. *Acta Sedimentologica Sinica* **33**, 665–78 (in Chinese with English abstract).
- Yin HQ, Zhou HR, Zhang WJ, Zheng XM and Wang SY (2016) Late Carboniferous to early Permian sedimentary-tectonic evolution of the north of Alxa, Inner Mongolia, China: evidence from the Amushan formation. *Geoscience Frontiers* **7**, 733–41.
- Yin JY, Chen W, Xiao WJ, Yuan C, Sun M, Tang GJ, Yu S, Long XP, Cai KD, Geng HY, Zhang Y and Liu XY (2015) Petrogenesis of Early-Permian sanukitoids from West Junggar, Northwest China: implications for Late Paleozoic crustal growth in Central Asia. *Tectonophysics* **662**, 385–97.
- Yu W, Shao ZG, Niu MLM and Su H (2022) Discovery of a Mesoproterozoic granite in the northern Alxa Block and its tectonic implication. *Geological Journal* **57**, 3706–20.
- Zhang BH, Zhang J, Zheng RG, Qu JF, Hui J, Zhao H, Zhao S, Niu PF, Zhang YP and Yun L (2022) Paleozoic tectonic evolution of the central part of the southern central Asian Orogenic Belt: constraints from the detrital zircon U–Pb ages and sedimentary characteristics. *Gondwana Research* **101**, 1–20.
- Zhang W, Pease V, Meng QP, Zheng RG, Wu TR and Chen Y (2017) Age and petrogenesis of late Paleozoic granites from the northernmost Alxa region, Northwest China, and implications for the tectonic evolution of the region. *International Journal of Earth Sciences* **106**, 1–18.
- Zhang W, Pease V, Meng QP, Zheng RG, Wu TR, Chen Y and Gan LS (2016) Discovery of a Neoproterozoic granite in the Northern Alxa region, NW China, its age, petrogenesis and tectonic significance. *Geological Magazine* **153**, 512–23.
- Zhao XC, Liu CY, Wang JQ, Zhang SH and Guan YZ (2020) Geochemistry, geochronology and Hf isotope of granitoids in the northern Alxa region, implications for the Late Paleozoic tectonic evolution of the Central Asian Orogenic Belt. *Geoscience Frontiers* **11**, 1711–25.
- Zhao ZH, Wang Q, Xiong XL, Niu HC, Zhang HX and Qiao YL (2009) Magnesian andesites in north Xinjiang, China. *International Journal of Earth Sciences* **98**, 1325–40.
- Zheng RG, Li JY, Xiao WJ and Wang LJ (2018) A new ophiolitic MÉLANGE containing boninitic blocks in Alxa region: implications for Permian subduction events in southern CAOB. *Geoscience Frontiers* **9**, 1355–67.
- Zheng RG, Wu TR, Zhang W, Feng JC, Xu C, Meng QP and Zhang ZY (2013) Geochronology and geochemistry of the Yagan granite in the northern margin of the Alxa block, constraints on the tectonic evolution of the southern Altai. *Acta Petrologica Sinica* **29**, 2665–75 (in Chinese with English abstract).
- Zheng RG, Wu TR, Zhang W, Xu C, Meng QP and Zhang ZY (2014) Late Paleozoic subduction system in the northern margin of the Alxa block, Altaids, geochronological and geochemical evidences from ophiolites. *Gondwana Research* **25**, 842–58.
- Zheng RG, Zhang J and Xiao WJ (2019) Association of Permian gabbro and granite in the Langshan, southern Central Asian Orogenic Belt: age, origin tectonic implications. *Lithos* **348–349**, 105174.
- Zhou LM, Wang R, Hou ZQ, Li C, Li XW and Qu WJ (2018) Hot Paleocene–eocene Gangdese arc: growth of continental crust in southern Tibet. *Gondwana Research* **62**, 178–97.
- Zhou XH, Sun M, Zhang GH and Chen SH (2002) Continental crust and lithospheric mantle interaction beneath North China: isotopic evidence from granulite xenoliths in Hannuoba, Sino-Korean craton. *Lithos* **62**, 111–24.
- Zhou YZ, Han BF, Xu Z, Ren R and Su L (2013) The age of the Proterozoic rocks in Yingba area in western Inner Mongolia: constraints on the distribution of the South Gobi micro-continent in the Central Asian orogenic belt. *Geological Bulletin of China* **32**, 318–26 (in Chinese with English abstract).